Geophysical Prospecting, 2007, **55**, 135–154

Constraints on velocity-depth trends from rock physics models

Peter Japsen,[1]* Tapan Mukerji[2] and Gary Mavko[2]

[1]*Geological Survey of Denmark and Greenland (GEUS), Øster Voldgade 10, DK-1350 Copenhagen n K, Denmark, and* [2]*Stanford Rock Physics Laboratory, Stanford University, California 94305, USA*

Received June 2005, revision accepted July 2006

ABSTRACT

Estimates of depth, overpressure and amount of exhumation based on sonic data for a sedimentary formation rely on identification of a normal velocity–depth trend for the formation. Such trends describe how sonic velocity increases with depth in relatively homogeneous, brine-saturated sedimentary formations as porosity is reduced during normal compaction (mechanical and chemical). Compaction is 'normal' when the fluid pressure is hydrostatic and the thickness of the overburden has not been reduced by exhumation. We suggest that normal porosity at the surface for a given lithology should be constrained by its critical porosity, i.e. the porosity limit above which a particular sediment exists only as a suspension. Consequently, normal velocity at the surface of unconsolidated sediments saturated with brine approaches the velocity of the sediment in suspension. Furthermore, porosity must approach zero at infinite depth, so the velocity approaches the matrix velocity of the rock and the velocity–depth gradient approaches zero. For sediments with initially good grain contact (when porosity is just below the critical porosity), the velocity gradient decreases with depth. By contrast, initially compliant sediments may have a maximum velocity gradient at some depth if we assume that porosity decreases exponentially with depth. We have used published velocity–porosity–depth relationships to formulate normal velocity–depth trends for consolidated sandstone with varying clay content and for marine shale dominated by smectite/illite. The first relationship is based on a modified Voigt trend (porosity scaled by critical porosity) and the second is based on a modified time-average equation. Baselines for sandstone and shale in the North Sea agree with the established constraints and the shale trend can be applied to predict overpressure. A normal velocity–depth trend for a formation cannot be expressed from an arbitrary choice of mathematical functions and regression parameters, but should be considered as a physical model linked to the velocity–porosity transforms developed in rock physics.

INTRODUCTION

A normal velocity–depth trend is a function describing how sonic velocity increases with depth in a relatively homogeneous, brine-saturated sedimentary formation when porosity is reduced during normal compaction (mechanical or chemical). Compaction is 'normal' when the fluid pres-sure of the formation is hydrostatic and the formation is at maximum burial depth, i.e. the thickness of the overburden has not been reduced by exhumation. The term baseline is frequently used as a synonym for a normal velocity–depth trend, typically to refer to reference trends established from a given database. The sonic velocity may be represented by the velocity V [m/s] or by transformations like transit time, $tt = 1/V \cdot 10^6$ [μs/m].

Velocity–depth studies are useful because they are based on easily accessible data with a wide lateral and vertical coverage, and can thus prescribe simple constraints on both physical and

*E-mail: pj@geus.dk

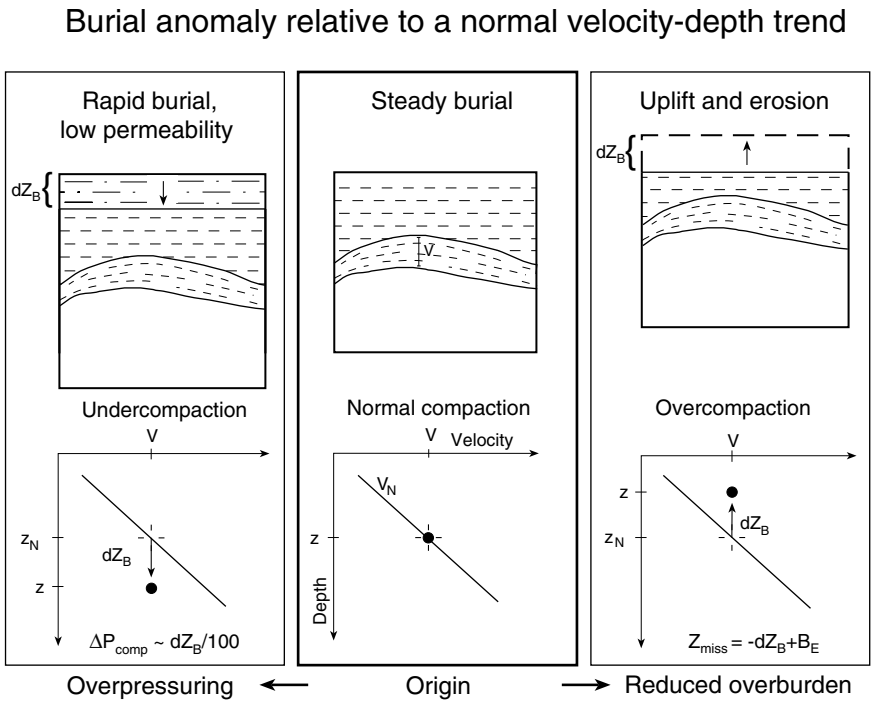

Figure 1 Burial anomaly dZ_B [m], relative to a normal velocity–depth trend V_N, for a sedimentary formation. In the North Sea Basin, burial anomalies of ±1 km for pre-Miocene formations result from late Cenozoic exhumation along basin margins and overpressuring due to rapid, late Cenozoic burial in the basin centre (cf. Figure 11). Rapid burial and low permeability cause undercompaction and overpressure ΔP_{comp} [MPa], and velocities that are low relative to depth (positive dZ_B) (cf. Equation 9). Exhumation due to uplift reduces the overburden thickness and causes overcompaction expressed as velocities high relative to depth (negative dZ_B); however, post-exhumational burial, B_E, will mask the magnitude of the missing section Δz_{miss}. The normalized depth z_N is the depth corresponding to normal compaction for the measured velocity (cf. Terzaghi's principle; Terzaghi and Peck 1968). Modified after Japsen (1998).

geological parameters because acoustic waves are affected by bulk properties as they propagate through the sediment. Disagreement between predicted and measured velocity at a given depth may indicate that a formation has become overpressured due to rapid burial (resulting in a lower velocity than expected) or that the overburden has been partially removed subsequent to maximum burial (resulting in a higher velocity than expected) (Fig. 1). A velocity–depth anomaly can also be measured along the depth axis as the burial anomaly dZ_B [m] (Japsen 1998). Velocity–depth trends are used for:

- estimating the amount of removed overburden ('uplift') relative to an overcompacted formation (e.g. Acheson 1963; Magara 1978; Bulat and Stoker 1987; Japsen 1993, 1998, 2000; Hillis 1995; Hansen 1996b; Heasler and Kharitonova 1996; Ware and Turner 2002; Corcoran and Doré 2005; Corcoran and Mecklenburgh 2005; Walford and White 2005; Mackay and White 2006);
- estimating overpressure due to undercompaction (e.g. Hottmann and Johnson 1965; Magara 1978; Chapman 1983; Japsen 1998, 1999; Winthaegen and Verweij 2003);
- converting traveltime to depth (e.g. Slotnick 1936; Japsen 1993; Al-Chalabi 1997b);
- determining background velocity – or the low-frequency model – for inversion of seismic data (e.g. Snieder *et al.* 1989);
- modelling the manner in which amplitude variation with offset (AVO) intercept and gradient change with increasing burial (e.g. Smith and Sondergeld 2001).

Rock-physics relationships, such as the empirical time-average of Wyllie *et al.* (1956), the relationships of Raymer *et al.* (1980) or the modified Voigt model (Nur *et al.* 1998), relate velocity to porosity for different rock types (cf. Dvorkin *et al.* 2002), but even though the concept of velocity–depth trends is as old as exploration geophysics (e.g. Slotnick 1936; Haskell 1941), few attempts have been made to constrain them for different lithologies, rather than just considering velocity–depth trends as fits of arbitrary functions to local data sets.

Chapman (1983) combined the time-average equation with the exponential decay of porosity with depth and thus derived an expression for the increase in shale velocity with depth that

is constrained by the velocity of the sediment at the surface and does not approach infinite velocity at depth. Bulat and Stoker (1987) and Hillis (1995) estimated baselines for different lithologies but did not consider that the physical properties of the rock influence the curvature of velocity–depth trends and that velocity is finite even at great depth. Japsen (1998, 1999, 2000) defined normal velocity–depth trends for chalk and shale in such a way that the predicted velocities agreed with those of recent deposits at the surface and that they did not approach infinity at depth. Velocity–depth anomalies relative to these trends were found to be in agreement with estimates of the amount of exhumation along the margins of the North Sea Basin, as well as with measurements of overpressure in the centre of this basin.

Much empirical and theoretical insight into the physics of rocks has been gained since the formulation of the time-average equation, and consequently the analysis of Bulat and Stoker (1987) and others can be refined. In this paper, we investigate how joining rock-physics V–ϕ models with the ϕ–z relationship during normal compaction for the rock in question can introduce sensible simple constraints on V–z trends (z is depth below the sea-bed or ground level [m], ϕ is porosity [fraction]). We find that the normal velocity at the surface for a given rock is constrained by its critical porosity, and demonstrate that differences in the initial grain contact in sandstone and shale influence the curvature of the velocity–depth trends for these sediments. We conclude that normal velocity–depth trends should be considered as physical models for specific lithologies.

ROCK-PHYSICS MODELS

Critical porosity

For most porous materials there appears to be a critical porosity ϕ_c, that separates mechanical and acoustic behaviour into two distinct domains (Nur *et al*. 1991; Chen and Nur 1994; Nur *et al*. 1998). By definition, ϕ_c is the porosity below which the mineral grains in a sediment become load-bearing. At porosities above ϕ_c, the sediment loses all rigidity and falls apart: the sediment is in suspension and the fluid phase is load-bearing. Critical porosity has also been called elastic percolation porosity (Feng and Sen 1985; Guéguen *et al*. 1997) or the precompaction porosity (Nolen-Hoeksema 1993).

The transition from suspension to solid is implicit in the empirical velocity–porosity relationship of Raymer *et al*. (1980). If critical porosity is exceeded at the time of initial deposition of grains, they are barely in contact and consequently have no rigidity (Guéguen and Palciauskas 1994). The value of ϕ_c is determined by sediment type, grain sorting and angularity at deposition, and can thus vary within the same rock type (Table 1a). The concept of critical porosity is developed for sediments saturated with brine, and the arguments presented here do not necessarily apply to aeolian sediments, for example. Critical porosity behaviour is a general geometric property and is a powerful constraint on theoretical models.

V–ϕ trajectories

The velocity (or effective modulus) of a rock with a given porosity and fluid composition always falls between the Voigt upper and the Reuss lower bounds, but its precise value depends on the geometric details of the grain-pore microstructure (see Appendix A). Stiffer pore shapes cause the velocity to be closer to the upper bound; softer or more compliant shapes cause the velocity to be lower (e.g. Mavko *et al*. 1998). When compaction and diagenesis reduce porosity and thus increase the elastic stiffness, data points for a given rock type and diagenetic history will fall along a specific path or trajectory (V–ϕ path) in a plot of velocity versus porosity.

Initially stiff rocks

The V–ϕ path is concave for rocks that show a strong increase in velocity for porosity reduction just below the critical porosity (curve V_N^{ss10} in Fig 2; e.g. consolidated sandstone), i.e.

$$\left(\frac{dV}{d\phi}\right)_{\phi\approx\phi_c} << 0, \quad \frac{d^2V}{d\phi^2} < 0.$$

A concave V–ϕ curve has a negative second derivative. The initial sensitivity to porosity reduction may be due to the growth and cementation of grain contacts (e.g. Dvorkin and Nur 1996), while mechanical compaction is limited. Here, we refer to such rocks as 'initially stiff rocks'.

Initially compliant rocks

The V–ϕ path is convex for rocks that show a weak increase in velocity for porosity reduction just below the critical porosity close to ϕ_c (curve V_N^{sh} in Fig 2; e.g. shale, chalk), i.e.

$$\left(\frac{dV}{d\phi}\right)_{\phi\approx\phi_c} \approx 0, \quad \frac{d^2V}{d\phi^2} < 0.$$

A convex V–ϕ curve has a positive second derivative. This initial insensitivity to porosity reduction may be attributed to dominance of compaction, poor sorting and growth of pore-filling cement. Here, we refer to such rocks as 'initially compliant rocks'.

Table 1 Parameters and velocity-depth models

a. Critical porosity and exponential porosity decay with depth

Lithology	Critical porosity[a] ϕ_c [%]	Compaction models, literature				Compaction model, applied	
		Area, depth data	ϕ_0 [%]	β [m]	Reference	ϕ_0 [%]	β [m]
Sandstone	40	North Sea, 2–3 km	49	3704	Sclater and Christie (1980)	40	4872
		Nigeria, 0.6–4.3 km	44	4631	Serra (1986)		
Shale	60–90	North Sea, 0.3–2.6 km	71	1961	Hansen (1996a)	71	1961
		North Sea, -	63	1961	Sclater and Christie (1980)		

b. Rock physical properties

Material	ϕ [%]	V_p [km/s]	V_s [km/s]	K [GPa]	μ [GPa]	ρ [g/cm^3]	Source
Quartz	-	6.04	4.12	36.6	45.0	2.65	Mavko *et al.* (1998)
Water	-	1.50	0	2.25	0	1	
At 4 km depth [b]							
Sandst. 0% clay	17.6	4.66	2.95	25.1	21.6	2.48	Han *et al.* (1986)
Sandst. 10% clay	17.6	4.15	2.47	21.7	14.5	2.38	Han *et al.* (1986)
Sandst. 20% clay	17.6	3.93	2.28	20.0	12.1	2.34	Han *et al.* (1986)
Sandst. 30% clay	17.6	3.72	2.09	18.3	10.0	2.29	Han *et al.* (1986)
At ϕ_c [c]		V_c		K_c		ρ_c	
Quartz	40	1.60	0	5.15	0	2.00	Equation (A-1)

c. Velocity-depth models

$V-z$ trend z [km]	V_N^{ss00} [d]	V_N^{ss10} [d]	V_N^{ss20} [d] V [km/s]	V_N^{ss30} [d]	V_N^{sh} [e]
0	1.55	1.58	1.59	1.60	1.55
1	3.07	2.80	2.68	2.58	2.10
2	3.83	3.44	3.27	3.11	2.71
3	4.32	3.86	3.66	3.47	3.32
4	4.66	4.15	3.93	3.72	3.87
z_i-z_{i+1} [km]			k [s^{-1}]		
0-1	1.52	1.22	1.10	0.97	0.55
1-2	0.76	0.64	0.59	0.54	0.61
2-3	0.49	0.42	0.39	0.35	0.61
3-4	0.34	0.29	0.27	0.25	0.55
0-4	0.78	0.64	0.59	0.53	0.58

[a] Critical porosities found by evaluation of velocity-porosity data (Nur *et al.* 1998; Mavko *et al.* 1998).

[b] Based on laboratory data and linear dependency of rock physical parameters on porosity. Porosity based on compaction models in Table 1a.

[c] Reuss bound (equation A-1).

[d] Sandstone model computed from the $V-\phi$ trend given by equation, the appropriate rock physical properties for 0, 10, 20 and 30% clay content (Table 1b) (A2) and the $\phi-z$ model for sandstone (Table 1a).

[e] Marine shale (equation 5).

COMPACTION TRENDS

Burial of sediment leads to initial compaction and reduction of porosity to less than ϕ_c. We therefore assume that critical porosity of the sediment is reached only at the surface when pressure remains hydrostatic. We make the important assumption that ϕ_0, the porosity at the surface of the sedimentary succession, is constrained by the critical porosity of the freshly deposited sediment, i.e.

$$\phi_0 \leq \phi_c. \quad (1)$$

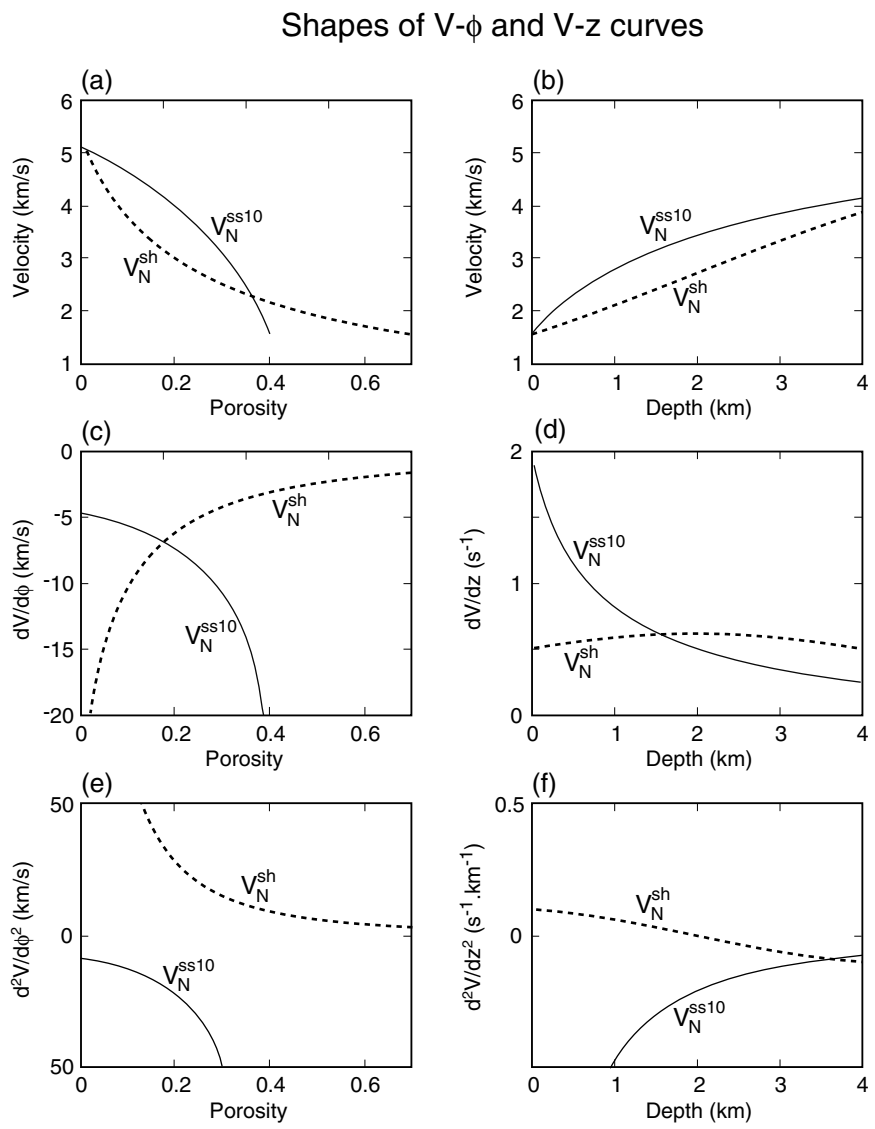

Figure 2 Shapes of V–ϕ and V–z curves for sediments characterized by initially stiff or initially compliant pore space (e.g. consolidated sandstone and marine shale, Figs 3 and 4). The two sediments have concave and convex V–ϕ trajectories, and thus $\mathrm{d}^2V/\mathrm{d}\phi^2$ for each type becomes negative and positive, respectively. The velocity gradient $k = dV/dz$ decreases with depth for the first type, while it has a maximum for the other type. (a) (c) and (e): V–ϕ trend and first and second derivatives with respect to ϕ. (b) (d) and (f): V–z trend and first and second derivatives with respect to z. The exponential ϕ–z relationships for both sediments are given in Table 1(a). V_N^{ss10}: modified Voigt model for sandstone, 10% clay content (equation (A2)). V_N^{sh}: marine shale trend (equations 5 and 6, V–ϕ and V–z relationships, respectively).

The geological interpretation of this statement is that, at least for clastics, the weak suspension state at critical porosity describes the sediment when it is first deposited, before compaction and diagenesis. The overall agreement between independent estimates of ϕ_c and ϕ_0 for different rock types supports the assumption that the limiting porosity at the surface is close to the critical porosity, e.g. for chalk $\phi_0 = 70\%$ (Scholle 1977) and $\phi_c = 65\%$ (Nur *et al*. 1998; cf. Fabricius 2003) (see Table 1a).

The porosity-reduction in sedimentary rocks during normal compaction has frequently been approximated by exponential functions (e.g. Athy 1930; Rubey and Hubbert 1959; Magara 1978; Sclater and Christie 1980; Hansen 1996a). Exponential functions have convenient mathematical properties and predict a physically constrained variation of porosity. Exponential porosity decay is a first-order approximation and thus does not include, for example, the onset of cementation below a certain depth. If we apply this approximation and set

porosity at the surface to ϕ_c, we obtain

$$\phi = \phi_0 e^{-z/\beta} = \phi_c e^{-z/\beta}, \quad (2)$$

where the constant β [m] is a measure of the rate of porosity decay. The assumption $\phi_0 = \phi_c$ allows us to link knowledge from rock physics with compaction trends.

NORMAL VELOCITY–DEPTH TRENDS

General conditions

We will consider velocity as a function of porosity and porosity as a function of depth, i.e.

$$V(z) = V[\phi(z)],$$

where z may range from the surface to infinite depth. The velocity–depth gradient, k [m/s/m = s^{-1}], can be calculated by differentiation of the above expression, i.e.

$$k = \frac{dV}{dz} = \frac{d}{dz} V[\phi(z)] = \frac{d}{d\phi} V(\phi) \frac{d}{dz} \phi(z), \quad (3)$$

showing that the shape of the V–z trend depends on the shape of the V–ϕ and ϕ–z curves. As both terms on the right are negative or zero, we get $k \geq 0$ (cf. Figure 2c).

We can set up three simple boundary conditions for $V(z)$ for $z = 0$ and $z \to \infty$:

- $V_0 \geq V_c$. The velocity of unconsolidated sediments at the surface, V_0, is constrained by the velocity at critical porosity, V_c, given by the Reuss average at ϕ_c (equation (A1)). This follows from equation (1). Thus V_0 will, in general, differ from the velocity of water (Tables 1b,c).
- $V_\infty \to V_m$. Since porosity at infinite depth approaches zero, the velocity V_∞ of the sedimentary rock at infinite depth approaches the velocity at zero porosity, the velocity V_m, of the matrix mineral at high pressure and temperature.
- $k \to 0$ for $z \to \infty$. The velocity–depth gradient must approach zero at infinite depth as velocity cannot increase beyond the finite value of V_m.

Assuming exponential form for ϕ–z trends

We can simplify the relationship between velocity and depth by introducing exponential porosity decay with depth (equation 2):

$$V(z) = V[\phi(z)] = V(\phi_0 e^{-z/\beta}).$$

The velocity–depth gradient is found by making the same substitution in equation (3):

$$k = \frac{dV}{d\phi} \cdot \frac{d\phi_0 e^{-z/\beta}}{dz} = \frac{dV}{d\phi}\left(-\frac{1}{\beta}\phi_0 e^{-z/\beta}\right) = -\frac{dV}{d\phi}\phi/\beta.$$

The proportionality between k and $dV/d\phi$ means that the shape of the V–z path reflects the shape of the V–ϕ path. We can compare V–z trends for rocks with different curvature in the V–ϕ plane by differentiating the above expression for k assuming exponential porosity-decay with depth (equation 2):

$$\frac{dk}{dz} = \frac{d}{dz}\left[-\frac{dV}{d\phi}\frac{\phi}{\beta}\right] = \frac{dV}{d\phi}\frac{d}{dz}\left[-\frac{\phi}{\beta}\right] - \frac{\phi}{\beta}\frac{d}{dz}\left[\frac{dV}{d\phi}\right]$$
$$= \frac{1}{\beta^2}\left(\frac{dV}{d\phi} + \phi\frac{d^2V}{d\phi^2}\right)\phi.$$

The first term on the right is negative for any rock, while the sign of the second term depends on the curvature of the V–ϕ path, i.e. positive or negative for rocks that are initially compliant or stiff, respectively (curves V_N^{sh} and V_N^{ss10} in Fig. 2e).

- For initially stiff rocks ($d^2V/d\phi^2 < 0$), we get $dk/dz < 0$, indicating that $k(z)$ decreases monotonously with increasing depth from the surface, i.e. with no local maxima for the velocity–depth gradient (curve V_N^{ss10} in Figs 2d,f). This decreasing velocity–depth gradient at shallow depths reflects the slowdown in the velocity increase, perhaps after the initial growth and cementation of grain contacts (see the sandstone case below; Fig. 3).
- For initially compliant rocks ($d^2V/d\phi^2 > 0$), dk/dz may become zero (curve V_N^{sh} in Figs 2d,f). Therefore, an increasing velocity–depth gradient at shallow depths may reflect the accelerated increase in velocity as mechanical compaction takes place, whereas the slow-down in porosity-reduction at depth leads to a decreasing velocity–depth gradient. Initially compliant rocks may thus have a maximum velocity gradient at an intermediate depth due to the combined effect of these two processes (see the shale case below; Fig. 4).

We investigate velocity–depth relationships for specific velocity–porosity trends in Appendix B and we discuss analytical functions that have been applied to represent the increase in ve-locity with depth in Appendix C (see also Table 2).

BASELINES FOR SANDSTONE AND SHALE ESTIMATED FROM NORTH SEA DATA

It can be difficult to estimate the normal velocity–depth trend for a formation because the formation may not easily be found under normally compacted conditions, e.g. the formation may either be undercompacted due to overpressuring or it may be

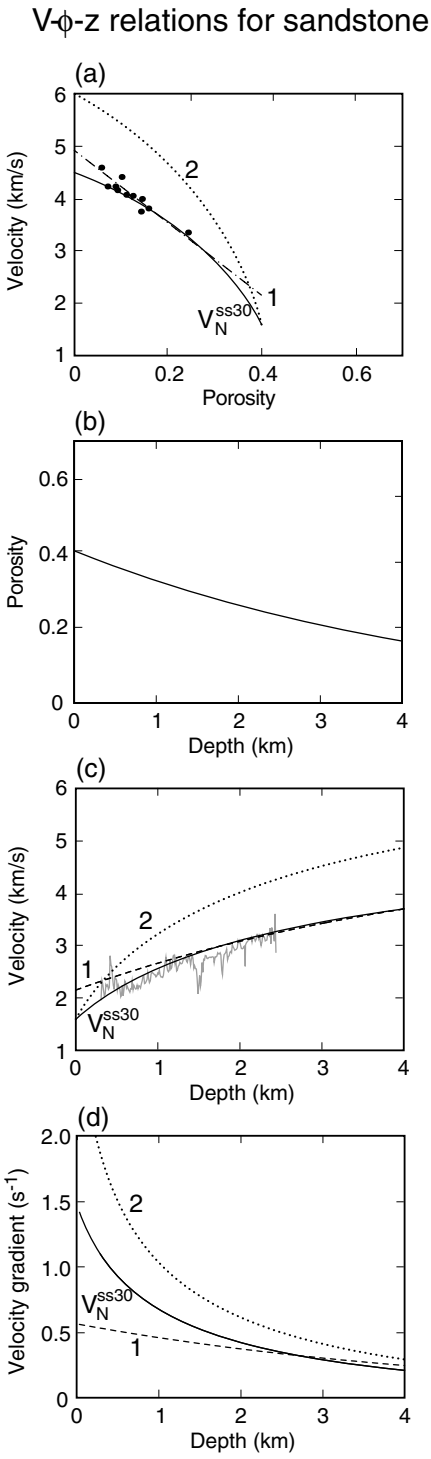

Figure 3 Sandstone; relationships between velocity, porosity, depth and velocity–depth gradient. A modified Voigt upper bound (V_N^{ss30}) represents the transition from sand to sandstone during normal compaction by constraining the porosity to vary between critical porosity and estimated porosity at a depth of 4 km (equation (A2)) (Nur *et al*. 1991). (a) V–ϕ trends and data points for clay content between 20 and 40% at 40 MPa confining pressure (cf. Table 1b) (Han *et al*. 1986); (b) ϕ–z trend based on models for the North Sea and Nigeria (Table 1a); (c) V–z trends resulting from elimination of ϕ in (a) and (b) and sonic log covering normally compacted, Cenozoic sandstones in the Kangâmiut-1 well, offshore SW Greenland (Rolle 1985); (d) k–z trends from (c). 1: linear trend from laboratory data; 2: modified Voigt trends from mineral properties at $\phi = 0$; V_N^{ss30}: modified Voigt trend from laboratory data, 30% clay content, anchor point at $\phi_{4\mathrm{km}}$.

overcompacted due to exhumation of its overburden (Fig. 1). It may, however, be possible to estimate the maximum burial of the formation independently: along the margins of the North Sea Basin, the amount of Cenozoic exhumation can be calculated from the burial anomaly of the thick and uniform Upper Cretaceous–Danian chalk relative to the normal velocity–depth trend for the chalk (Japsen 1998, 2000). Baselines can be more easily traced in plots of velocity versus pre-exhumation depths because the formations underlying the chalk were at maximum burial at more locations prior to the exhumation (Fig. 5). Data points at shallow depth relative to the baseline may thus represent locations where the formation experienced maximum burial during the Mesozoic (cf. Japsen 2000).

Normal velocity–depth trends for sandstone and shale were established by Japsen (2000) from a regional database of interval velocities estimated in UK and Danish wells in the North Sea Basin (cf. Hillis 1995). The wells have interval velocities from a marine Jurassic shale (the F-1 Member of the Lower Jurassic Fjerritslev Formation), from the Triassic redbeds of the Bunter Sandstone or the Bunter Shale, as well as from the North Sea Chalk. The Triassic redbeds were deposited in a supratidal or continental environment during a hot, semiarid climate (Bertelsen 1980; Johnson *et al*. 1994). The Fjerritslev Formation was deposited in a marine environment (Michelsen 1989) and its clay mineralogy is dominated by smectite/illite in distal parts of the basin (H. Lindgreen, pers. comm. 2000).

A baseline for sandstone based on data for Triassic formations

Bunter Shale

The plot of velocity versus pre-exhumation depths for the Bunter Shale in Fig. 6(b) shows a reasonably well-defined trend of data points at maximum burial ($2.6 < V < 4.8$ km/s). By

Table 2 Functional forms of velocity-depths trends

Linearity	$V(z)$ or $tt(z)$ (equation no.)	Degrees of freedom	$V(0)$	$k = \mathrm{d}V/\mathrm{d}z$	$z \to \infty$		Selected references
					$k \to$	$V \to$	
$V - z$	$V = V_0 + k \cdot z$ (C-1)	2	V_0	k	k	∞	Slotnick (1936), Bulat and Stoker (1987)
$tt - z$	$tt = tt_0 + q \cdot z$ (C-2)	2	$1/tt_0$	$-q \cdot V^2$	∞[b]	∞[b]	Hillis (1995), Al-Chalabi (1997a)
$\ln(tt) - z$	$tt = tt_0 \cdot e^{-z/b_1}$ (C-3)	2	$1/tt_0$	V/b_1	∞	∞	Magara (1978), Hansen (1996b)
$\ln(V) - \ln(z)$	$V = c \cdot z^{1-n}$, $0.83 < n < 1$ (C-4)	2	0	$(1-n) \cdot V/z$	0	∞	Faust (1951), Acheson (1963)
$\ln(tt - tt_\infty) - z$, $\ln(tt - tt_\infty) - \phi$[e]	$tt = (tt_0 - tt_\infty)e^{-z/b_2} + tt_\infty$ (C-5)	3	$1/tt_0$	$(\mathrm{V} - tt_\infty \cdot V^2)/b_2$[c]	0	$1/tt_\infty$	Chapman (1983), Al-Chalabi (1997a), Japsen (1999)
$V - z$, N segments	$V = V_{0\mathrm{i}} + k_\mathrm{i} \cdot z$, $z_{\mathrm{ai}} < z < z_{\mathrm{bi}}$ (C-6)	$2N$	V_{01}	k_i	-[a]	-[a]	Japsen (1998, 2000)
$\ln(V_\infty - V) - z$, $\ln(V_\infty - V) - \ln(\phi)$[e]	$V = V_\infty - (V_\infty - V_0)e^{-z/b_3}$ (B-2)[d]	3	V_0	$(V_\infty - V)/\mathrm{b}_3$	0	V_∞	This paper

Units of model parameters: b_1, b_2, b_3, z [m], c, V, V_0, V_∞ [m/s], k [s^{-1}], q [$\mathrm{s/m}^2$], tt, tt_0, tt_∞ [s/m], n [−].

[a] Arbitrary, depending on actual parameters.

[b] For $z \to -tt_0/q$.

[c] Maximum velocity gradient for $z = b_2 \cdot \ln[(tt_0 - tt_\infty)/tt_\infty]$.

[d] Constrained approximation to the modified Voigt trend based on exponential porosity-decay (equation A2).

[e] Combined with exponential porosity decay with depth.

contrast, the plot of velocity versus present depth in Fig. 6(a) reveals no clear trend. Some data points are plotted above the trend in Fig. 6(b) and thus represent areas where the Bunter Shale was at maximum burial prior to Cenozoic exhumation or areas of anomalous lithology.

The trend of data points at maximum burial reveals a slight curvature that reflects the decrease in the velocity gradient with depth, and this trend is approximated by three linear segments plus a fourth segment that connects the observed trend with a physically reasonable velocity at the surface. The normal velocity–depth trend for the Bunter Shale, V_N^B, can be approximated by the following expression (Japsen 2000):

$$\begin{aligned} V_\mathrm{N}^\mathrm{B} &= 1550 + 0.6z, && 0 < z < 1393\,\mathrm{m}, \\ V_\mathrm{N}^\mathrm{B} &= -400 + 2z, && 1393 < z < 2000\,\mathrm{m}, \\ V_\mathrm{N}^\mathrm{B} &= 2600 + 0.5z, && 2000 < z < 3500\,\mathrm{m}, \\ V_\mathrm{N}^\mathrm{B} &= 3475 + 0.25z, && 3500 < z < 5300\,\mathrm{m}. \end{aligned} \tag{4}$$

The gradient is 2 s^{-1} for depths around 2 km, from where it decreases gradually with depth to 0.5 and then to 0.25 s^{-1} 0. The gradient is taken to be 0.6 s^{-1} in the upper part in order to arrive at a physically reasonable velocity at the surface.

Bunter Sandstone

The plot of velocity versus pre-exhumation depths for the Bunter Sandstone in Fig. 7(b) has a scattered trend of data at maximum burial that coincides with the trend for the Bunter Shale ($3.0 < V < 4.3$ km/s), and equation (4) is thus considered as an approximation for the observed Bunter Sandstone trend. See the section 'V–ϕ–z relationships for consolidated sandstone' for further discussion.

A shale trend based on data for a Jurassic formation

The plot of velocity versus pre-exhumation depths for the marine Lower Jurassic shale in Fig. 8(b) shows a well-defined trend of data points at maximum burial ($2.6 < V < 3.6$ km/s). A number of data points are plotted above the trend and presumably represent either areas where the shale was at maximum burial prior to Cenozoic exhumation or areas of anomalous lithology. The normal velocity–depth trend for the marine shale, V_N^sh, can be approximated by a constrained exponential

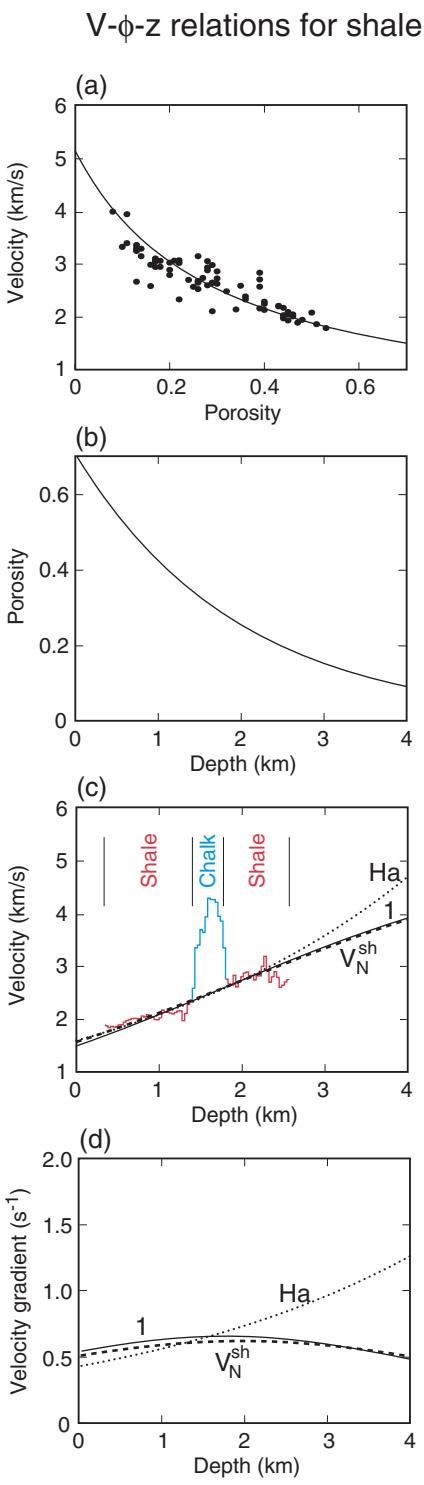

Figure 4 Shale; relationships between velocity, porosity, depth and velocity–depth gradient based on North Sea data. The constrained transit-time–depth model derived from log and core data (line 1) corresponds to a normal velocity–depth trend derived from interval velocity data (V_N^{sh}). (a) V–ϕ trend based on log and core data (equation 6; Hansen 1996a); (b) ϕ–z trend based on transit times converted by equation (6) (Table 1a; Hansen 1996a); (c) V–z trends and sonic log from normally compacted sediments (1.1 km Cenozoic shale, 0.3 km mainly Mesozoic chalk and 0.8 km Mesozoic shale; Norwegian well 17/10−1; cf. Olsen 1979; Hansen 1996b); (d) k–z trends from (c). 1: trend resulting from elimination of ϕ in (a) and (b) (equation 7); Ha: Hansen (1996b) (exponential tt–z trend, equation 8); V_N^{sb}: trend for marine shale dominated by smectite/illite (equation 5; Japsen 1999, 2000).

transit-time–depth model of the form given by equation (C5) (Japsen 2000):

$$V_N^{sh} = 10^6/(460e^{-z/2175} + 185). \quad (5)$$

The trend fulfils reasonable boundary conditions at the surface and at infinite depth, $V_0 = 1550$ m/s and $V_\infty = 5405$ m/s, and it is well-defined at depths where velocity–depth data for normally compacted shale can be difficult to identify ($2 < z < 4$ km). The trend has a maximum velocity–depth gradient of 0.6 s^{-1} at $z = 2.0$ km. See the section 'V–ϕ–z relationships for shale' for further discussion.

The depth shift between the observed trends for the Bunter and for the marine shale exceeds 1 km for $V > 3$ km/s. This shift must be related to physical differences between the two lithologies that have the word 'shale' in common because an explanation related to a previous greater burial for the data points defining the Bunter trend than for the marine shale trend is not compatible with the geology of the area (see Japsen 2000).

CONSTRAINTS ON VELOCITY–DEPTH RELATIONSHIPS FOR SANDSTONE AND SHALE

Here we study the effect of porosity reduction on velocity in both the V–ϕ plane and the V–z plane for rock types with depth-dependent compaction such as consolidated sandstone and shale. By estimating V–ϕ and ϕ–z relationships for these lithologies, we can eliminate the dependence on ϕ in order to find likely V–z trends that we can compare with the North Sea baselines described in the preceding section. S-wave velocity may be predicted from V (P-wave velocity) based on empirical relationships for sandstone or shale (e.g. Han *et al.* 1986; Greenberg and Castagna 1992).

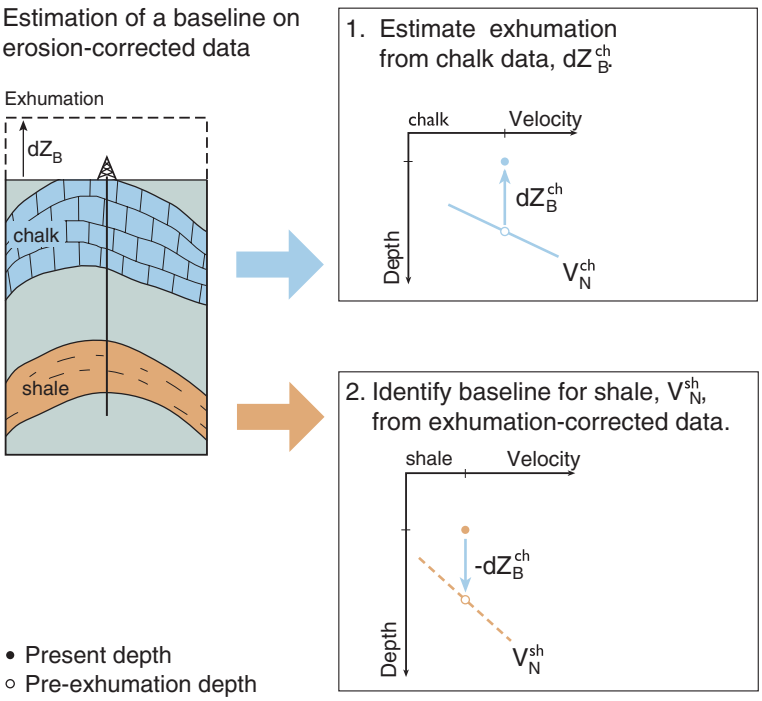

Figure 5 Identification of a normal velocity–depth trend for shale based on data from wells where Cenozoic exhumation can be estimated from velocity–depth data for the overlying North Sea chalk. Maximum burial is assumed to have occurred during the Cenozoic for both layers. 1 Estimate the Cenozoic exhumation in each well as the burial anomaly of the chalk, dZ_B^{ch}, relative to the chalk baseline, V_N^{ch}. 2 Identify the baseline, V_N^{sh}, for the shale unit by plotting velocity data versus depths corrected for exhumation as estimated by the chalk data. The shale baseline can be traced more easily because the shale was at maximum burial at more locations prior to Cenozoic exhumation.

V–ϕ–z relationships for consolidated sandstone

V–ϕ model

We construct modified Voigt upper bounds to describe the V–ϕ trend for consolidated sandstone with varying clay content during normal compaction (Han *et al*. 1986; Nur *et al*. 1991). The velocity varies between two end-members (equation (A2)): the maximum-porosity end-member for the mineral suspension at critical porosity (ϕ_c, V_c) (equation (A1)) and the minimum-porosity end-member (anchor point) representing maximum compaction for practical purposes, i.e. the porosity estimated at a depth of 4 km (ϕ_{4km}, V_{4km}) (Table 1a; curve V_N^{ss10} in Fig. 3a). We calculate rock properties for consolidated sandstones with clay contents of 0, 10, 20 and 30%, using $\phi_{4km} = 17.6\%$, from Han's empirical relationships based on a data set with mean porosity 16% (Table 1b) (Han *et al*. 1986).

This modified Voigt model is appropriate where data extend over depths ranging from partially consolidated shallow rocks to deeper well-consolidated rocks. In such situations, diagenesis is the dominant control over the V–ϕ trend, and the modified Voigt model seems to capture this behaviour. However, in cases where data all come from similar diagenetic ages, such as from a selected reservoir zone within a relatively narrow depth range, variations in texture, sorting and clay content dominate the V–ϕ trend, and models other than the modified Voigt are more appropriate (e.g. Dvorkin and Nur 1996).

ϕ–z model

Sclater and Christie (1980) suggested an exponential porosity–depth trend for sandstones in the North Sea, constrained by a surface porosity of 49% estimated for sand in Holocene beach and dune deposits by Pryor (1973). This value is above the surface value of 41% for river-bar sediments given by Pryor (1973), and above the critical porosity for clean and well-sorted sand, $\phi_c = 40\%$ (Nur *et al*. 1998). Furthermore, a surface porosity of 44% for sandstones was found by fitting an exponential decay function with porosities based on density log data (Serra 1986). Both trends, however, indicate similar porosities at depth, i.e. a mean value of $\phi_{4km} = 17.6\%$. We calculate the exponential decay constant (β in equation 2) for that value and $\phi_0 = 40\%$, and do not include the influence of clay content (Fig. 3b; Table 1a).

Resulting V–z model

V–z trends for sandstone are found by eliminating ϕ from the above two models (curve V_N^{ss30} in Fig. 3c; equations (A2) and (2)). The modified Voigt model defined by the minimum-porosity anchor point has a V–z gradient that decreases monotonously from values greater than 1 s^{-1} for $z < 0.4$ km and 30% clay content (Fig. 3d; Table 1c). Reduction of the clay content leads to higher velocity and velocity gradient (Fig. 9).

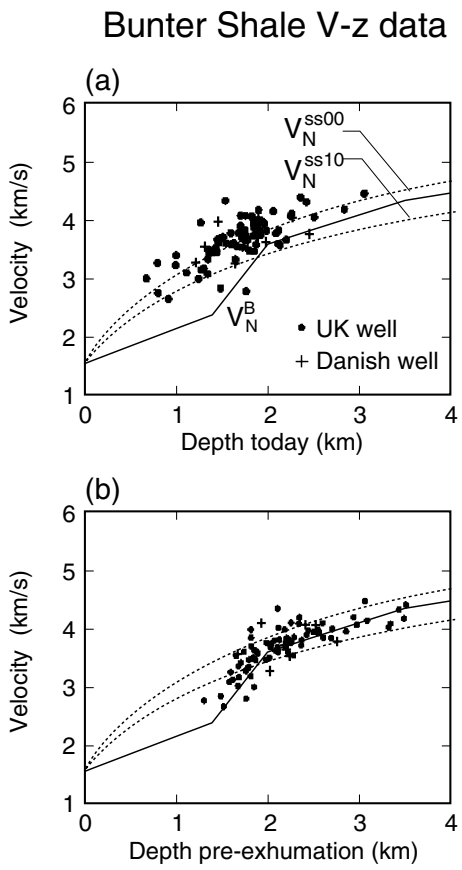

Figure 6 Plot of interval velocity versus midpoint depth for the Lower Triassic Bunter Shale. The Bunter model, V_N^B (equation 4) can be traced more easily if present depths are corrected for the Cenozoic exhumation in each well (Figure 5). Note the agreement between the Bunter trend and the modified Voigt model for sandstone below a depth of approximately 2 km. (a) Present-day depth below top of sediments; (b) depth prior to exhumation estimated by correcting present depths by the chalk burial anomaly in each well. One data point constrains V_N^B for a pre-exhumation depth of 5.5 km . $V_N^{ss}00$, $V_N^{ss}10$: modified Voigt models for sandstone, 0–10% clay content (equation (A2)). Modified after Japsen (2000).

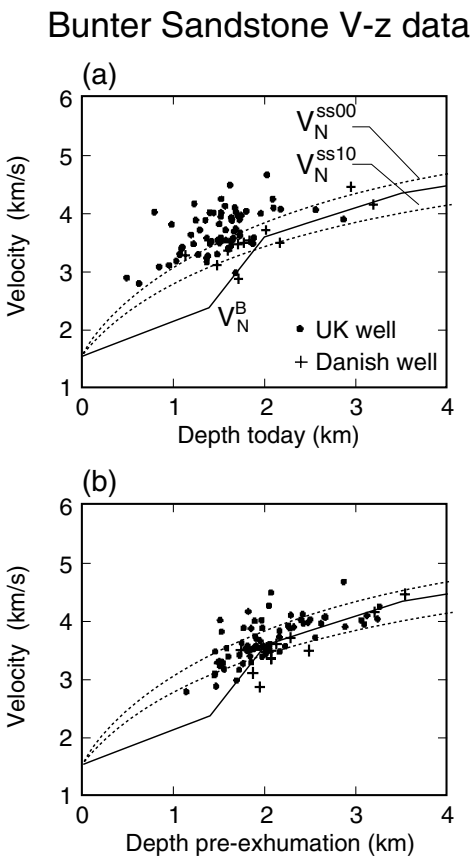

Figure 7 Plot of interval velocity versus midpoint depth for Bunter Sandstone. The Bunter model, V_N^B (equation 4), follows the scattered trend of the Bunter Sandstone data in the plot of depths corrected for exhumation in each well. (a) Present-day depth below top of sediments; (b) depth prior to exhumation estimated by correcting present depths by the chalk burial anomaly in each well. Three data points are plotted close to for a pre-exhumation depths of approximately 5 km . $V_N^{ss}00$, $V_N^{ss}10$: modified Voigt models for sandstone, 0–10% clay content (equation (A2)). Modified after Japsen (2000).

We can approximate the modified Voigt model by a modified velocity-average equation (equation (B2)).

If we compare the modified Voigt model with the normal trend for the Bunter Shale and Sandstone (Figs 6 and 7), we see that the Bunter trend – and most data points corrected for exhumation – are plotted between the sandstone models for 0% and 10% clay content for depths below approximately 2 km. The match between the modified Voigt model and the data points for the Bunter Sandstone supports the application of the modified Voigt model for sandstone (Fig. 3) as well as the estimation of the amount of exhumation by means of chalk velocities (Fig. 5).

The match between the modified Voigt model and the data points for the Bunter Shale suggests that the lithology of the Bunter Shale is dominated by quartz in the wide area covered by the data set (southern and eastern North Sea Basin). Consequently, the term 'Shale' seems to be an indication of grain size rather than of mineralogy.

The low velocities of the Bunter trend relative to the modified Voigt model at shallow depths may be explained by slow porosity-reduction in the Bunter Shale and Sandstone due to mechanical compaction above approximately 2 km, followed by a more rapid reduction due to the onset of quartz cementation below that depth (cf. Bjørlykke and Egebjerg 1993; Lander and Walderhaug 1999).

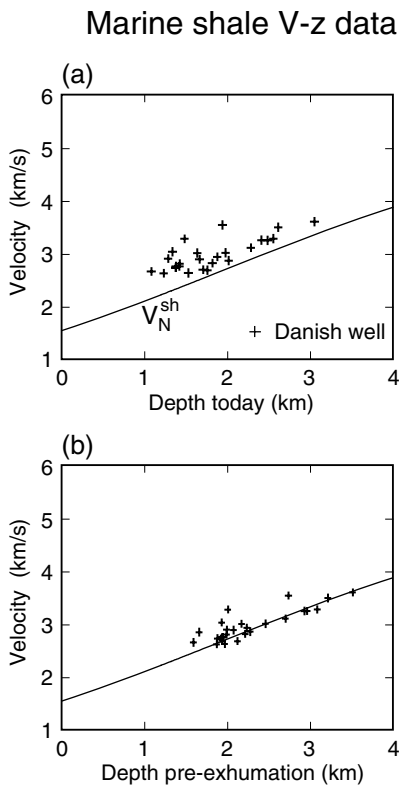

Figure 8 Plot of interval velocity versus midpoint depth for a marine Lower Jurassic shale (F-1 Member of the Fjerritslev Formation). The shale trend, V_N^{sh} (equation 5), can be traced more easily if present depths are corrected for Cenozoic exhumation in each well. (a) Present-day depth below top of sediments; (b) depth prior to exhumation estimated by correcting present depths by the chalk burial anomaly in each well. Modified after Japsen (2000).

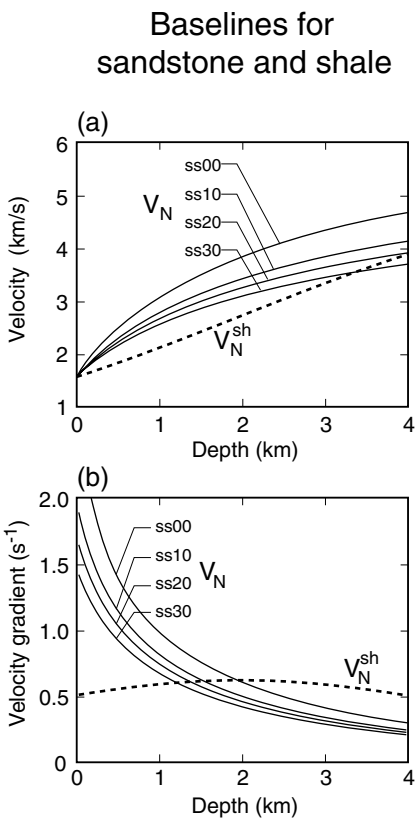

Figure 9 Composite plot of normal velocity–depth trends for sandstone and shale. The velocity of shale is predicted to be lower than that predicted for sandstone with a 30% clay content for $z < 4$ km. The velocity gradient for sandstone is predicted to decrease with depth whereas that of shale has a maximum at an intermediate depth. (a) V–z trends; (b) k–z trends. V_N^{sh}: marine shale trend (equation 5). $V_N^{ss00} - V_N^{ss30}$: modified Voigt models for sandstone, 0−30% clay content (equation (A2)).

The velocity–depth relationships for the Triassic Bunter Sandstone established by Bulat and Stoker (1987) and Hillis (1995) predict velocities at intermediate depths that are in agreement with the modified Voigt model for sandstone with 10% clay (e.g. $z \approx 2$ km; curves B&S, H and V_N^{ss10} in Fig. 10a). However, only the modified Voigt model complies with reasonable boundary conditions at the surface and at infinite depth (Fig. 10b). By contrast, the Bunter Sandstone model of Hillis (1995) predicts that the velocity–depth gradient increases towards infinity (cf. Equation (C2)). Consequently, exhumation may be underestimated by more than 500 m when this unconstrained sandstone trend is applied for velocities greater than 3.7 km/s compared to the modified Voigt model presented here. Underestimation by such amounts, which is only due to an unconstrained formulation of the baseline, is considerable compared to, for example, the amount of Cenozoic exhumation of the North Sea Basin that reaches approximately 1 km where the Upper Cretaceous Chalk is truncated (Japsen 1998, 2000).

V–ϕ–z relationships for shale

V–ϕ model

Hansen (1996a) calculated porosities from grain densities measured on cuttings and sidewall cores and from bulk densities estimated from density logs for Cretaceous-Cenozoic shales in three wells on the Norwegian Shelf. Corresponding transit times were determined by averaging sonic log values near the sampling depth. A modification of the Wyllie *et al*. (1956) time-average equation yielded a good fit for this data set (Fig. 4a) (Hansen 1996a). The modified time-average equation is in the form of equation (B1) where $1/\phi_c$ is substituted by a correction factor C_P. Hansen (1996a) found

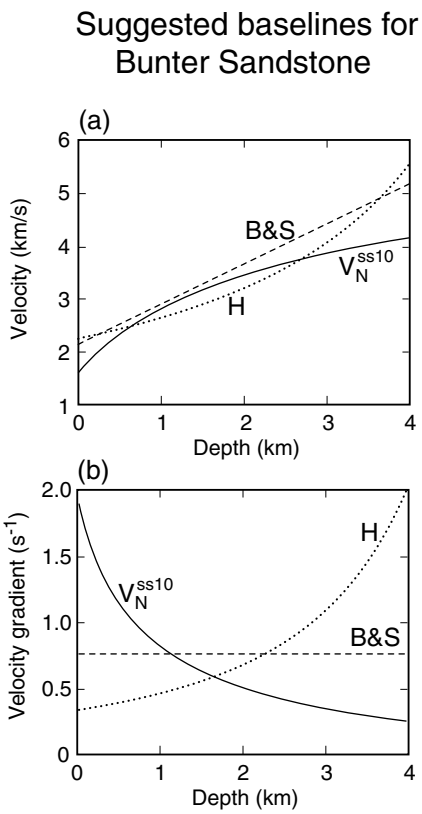

Figure 10 Comparison of suggested velocity-depth trends for the Triassic Bunter Sandstone, North Sea, with the modified Voigt model for sandstone with 10% clay (V_N^{ss10}). The two trends (B&S and H) show behaviour similar to the Voigt model at intermediate depths for which the trends were derived. Only the velocity gradient of the Voigt model converges towards zero at great depth. Data for the Bunter Sandstone are shown in Figure 7 (cf. Japsen 2000). (a) V–z trends; (b) k–z trends. B&S: Bulat and Stoker (1987) (linear V–z trend, cf. equation (C1)). H: Hillis (1995) (linear tt–z trend, cf. Equation (C2)). V_N^{ss10}: modified Voigt model for sandstone, 10% clay content (equation (A2)).

$C_P = 1.57$ ($\phi_c = 64\%$; $V_c = 1610$ m/s; $V_m = 5155$ m/s), and

$$tt = 670\phi + 194. \quad (6)$$

According to Hansen (1996a), differences in the determination of shale porosity are the main causes of differences between this result and the V–ϕ relationships for shale of Magara (1976), Issler (1992) and Liu and Roaldset (1994).

ϕ–z model

Hansen (1996a) calculated shale porosities from transit times based on the above tt–ϕ relationship for normally compacted Cretaceous-Cenozoic shale intervals in 29 wells on the Norwegian Shelf. Exponential and linear ϕ–z trends were fitted to the data, giving $\phi_0 = 71\%$ and 62%, respectively, which are in reasonable agreement with $\phi_c = 64\%$ indirectly determined by equation (6) (Fig. 4b; Table 1a).

Resulting V–z model

The expression resulting from combining the V–ϕ trend of equation (6) with the suggested exponential ϕ–z relationship (Hansen 1996a; Table 1a) is a constrained, transit-time–depth model (equation (C5); curve 1 in Fig. 4c):

$$tt = 676e^{-z/1961} + 194. \quad (7)$$

Hansen (1996b), however, chose to fit a simple, transit-time—depth model (equation (C3)) to data from normally compacted Jurassic-Miocene shale intervals in 32 wells on the Norwegian Shelf ($0.4 < z < 2.8$ km):

$$tt = 627e^{-z/3704}. \quad (8)$$

This equation predicts that the velocity approaches infinity at depth, and the two above trends are 0.8 km apart for $V =$ 4 km/s (curve Ha in Fig. 4c). By contrast, the shale trend of Japsen (2000) given by equation (5) (curve V_N^{sh} in Fig. 4d, Table 1c) is almost identical to that given by equation (7). Furthermore, it is less than 100 m apart from the trend of Hansen (1996b) for $z < 2.4$ km, which is the interval that covers most of the Cenozoic shale data.

Scherbaum (1982) presented a baseline for Lower Jurassic shale in the north-west German Basin, and this trend is within 100 m of that given by equation (5) for the adjacent Danish Basin for $z < 4$ km. Corcoran and Mecklenburgh (2005) estimated a shale trend of the same form as equation (5), based on regression of sonic log data for normally compacted, Jurassic-Cenozoic shale in the Rockall and Porcupine Basins. Inclusion of data from non-shale sediments in the analysis of Corcoran and Mecklenburgh (2005) may have caused their trend to be, on average, 497 m shallower than the trend given by equation (5) for a given velocity and $z < 4$ km. Thus there is uncertainty related to the identification of a uniform lithology for which the baseline is defined and to the selection of data for similar formations for which exhumation is to be determined. Shale trends based on data from the Gulf Coast area match that given by equation (5) at intermediate depths, from where most of the Cenozoic shale data originate ($0.5 < z < 1.5$ km). Few details are, however, given about the derivation of the Gulf Coast shale trends (e.g. Hottmann and Johnson 1965; Chapman 1983).

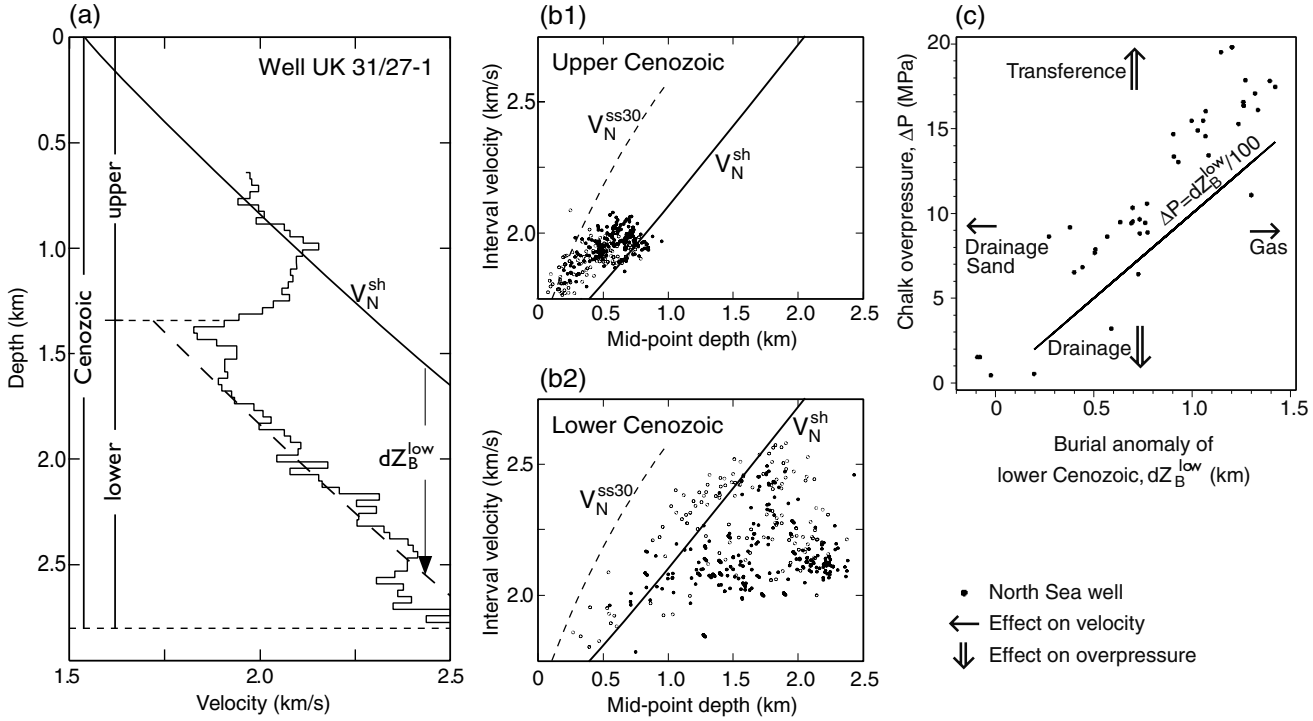

Figure 11 Prediction of overpressure in the North Sea from interval velocities of the Cenozoic deposits (excluding the Danian) (cf. Figure 1). (a) Sonic log where low velocities reveal undercompaction of the lower Cenozoic sediments corresponding to measured overpressure in the underlying chalk. (b1) and (b2) Interval velocity versus depth to the midpoint of the upper and lower Cenozoic deposits, respectively, for 322 North Sea wells. (c) Burial anomalies for the lower Cenozoic sediments (dZ_B^{low}) versus chalk formation overpressure (ΔP) in North Sea wells. The upper Cenozoic deposits are close to normal compaction whereas velocity–depth anomalies for the lower Cenozoic sediments outline a zone of undercompaction in the central North Sea. The deviations from the trend line in (c) are due to the non-compactional sources that add to the chalk overpressure from below (transference; cf. Osborne and Swarbrick 1997), the easier drainage from the more shallow Cenozoic section and sandy lithology ($\Delta P = \mathrm{d}Z_B/100$; equation 9). The burial anomalies are calculated relative to the shale trend given by equation (5). Depths below top of sediments. V_N^{ss30}: modified Voigt model for sandstone, 30% clay content (equation (A2)). V_N^{sh}: marine shale trend (equation 5). Modified after Japsen (1998, 1999, 2000).

Overpressure prediction from shale velocities

Overpressure in the central North Sea was successfully predicted from velocity–depth anomalies for the Cenozoic succession, relative to a normal velocity–depth trend for shale close to that given by equation (5) (Fig. 11; Japsen 1999). Investigation of interval velocities from almost 1000 wells revealed basin-wide differences in the physical properties of the Cenozoic deposits related to disequilibrium compaction below the mid-Miocene unconformity in the central North Sea (cf. Rubey and Hubbert 1959; Osborne and Swarbrick 1997).

The overpressure of an undercompacted rock, ΔP_{comp}, is proportional to the burial anomaly, dZ_B [m] (Fig. 1). Based on North Sea data, Japsen (1998) found that

$$\Delta P_{\mathrm{comp}} \approx dZ_B/100[\mathrm{MPa}], \qquad (9)$$

which means that a burial anomaly of 1000 m may reflect overpressure due to undercompaction of 10 MPa. In Fig. 11(c), we compare the degree of undercompaction of the lower Cenozoic succession in the North Sea, expressed by its burial anomaly dZ_B^{low}, with pressure data from the underlying chalk, ΔP_{ch}, because pressure measurements from the lower Cenozoic shales are rare in the central North Sea. We observe that ΔP_{ch} is proportional to dZ_B^{low}, and is of the order of the overpressure predicted by equation (9). This indicates that the burial anomaly for the lower Cenozoic succession relative to the shale trend given by equation (5) is a measure of overpressure due to undercompaction.

Comparison of *V–z* models for sandstone and shale

The velocity at the surface varies little for the sandstone and shale models presented here (approximately 1.6 km/s;

Table 1c; Fig. 9). However, different velocity gradients during normal compaction lead to a considerable range of velocities at a burial depth of 1 km for these models: sandstone velocities range from 2.6 to 3.1 km/s (30–0% clay content), while that of shale is predicted to be 2.1 km/s. For the models in Fig. 9, we predict the velocity of marine shale to be lower than that for sandstone with a clay content below 30% for $z < 3.5$ km.

The shapes of the velocity–depth trends for sandstone and shale differ markedly at shallow depth as indicated by the much higher velocity gradient for sandstone than for shale (1–1.5 s^{-1} as opposed to 0.55 s^{-1}, respectively, for z increasing from 0 to 1 km). Whereas the gradient for the sandstone trends decreases monotonously with depth, that for shale has a maximum value of 0.62 s^{-1} for $z = 2.0$ km. However, the velocity gradients are all close to 0.5 s^{-1} for the sandstone and shale models at intermediate depths.

DISCUSSION

Identification of a normal velocity–depth trend from basin-wide well data involves three steps of generalization, and this may explain differences among trends suggested for identical units by different authors. First, the model should be established for formations that are relatively homogeneous with regard to macroscopic acoustic properties, e.g. sandstone units of equal clay content or marine shale dominated by smectite/illite. Second, the trend should reflect normal compaction, but burial anomalies of ±1 km relative to the trend may be expected as the result of over- and undercompaction (Figs 1 and 11). Third, the mathematical formulation of the normal velocity–depth trends should be constrained by knowledge from rock physics.

Unconstrained trend lines fitted to local velocity–depth data may be useful for estimating the onset of overpressure or for predicting velocity within a limited depth range. However, a normal velocity–depth trend that complies with the above criteria is a prerequisite for estimating absolute values of depth, overpressure and the amount of exhumation based on sonic data for a sedimentary formation. Estimates of previous depth of burial (and hence exhumation) should thus be based on velocity data and models for specific lithologies: for example, for $V = 3$ km/s, the depth of normal compaction varies by up to 1 km, depending on whether the lithology is assumed to be shale or pure sandstone (Fig. 9). Consequently, the constrained, exponential tt–z trend given by equation (C5) that implies a V–ϕ relationship characteristic of a marine shale, should only be considered as a reference for sand/shale series (e.g. Heasler and Kharitonova 1996), for Triassic redbeds (e.g. Ware and Turner 2002) or for undefined lithologies along a seismic line (Walford and White 2005; Mackay and White 2006) (see Appendix B).

Normal compaction may be a difficult condition to prove because we do not always know if formation pressure is hydrostatic (e.g. in shale) or if a formation has been buried deeper prior to exhumation. If, for instance, a formation is exhumed, the observed minimum velocity at the surface may be mistaken for the normal velocity of the formation at zero depth prior to burial. These effects led Faust (1951) to suggest that the velocity for sand-shale sections was proportional to $(zT)^{1/6}$, where T is geological time in years (cf. Equation (C4)). Acheson (1963), however, realized that the apparent age effect observed by Faust (1951) could be explained by exhumation.

Japsen (1999) suggested that a shale trend close to that given by equation (5) could be applied more widely to marine shale dominated by smectite/illite and, thus, possibly to the Cenozoic shales in, for example, the Gulf Coast area. Illite and smectite are the main components of marine shale, making up 70% of the clay minerals in the major ocean basins today, and the shale of the Ceno-zoic deposits of the North Sea Basin and that in the Gulf Coast area are also dominated by smectite/illite (Weaver 1989). The validity of the baseline for marine shale given by equation (5) is indicated firstly by the successful prediction of overpressure in the North Sea (Fig. 11), secondly by the corre-spon-dence between this baseline and other suggested shale lines over significant velocity ranges (Scherbaum 1982; Hansen 1996b) and finally, by the fact that the trend is constrained by V–ϕ–z relationships for shale (Fig. 4).

CONCLUSIONS

The formulation of a normal velocity–depth trend for a formation is not an arbitrary choice of mathematical functions and regression parameters. The trend should be considered as a physical model of how the sonic velocity of a given lithology increases as porosity is reduced during burial and normal compaction in a sedimentary basin. We have investigated the properties of normal velocity–depth trends for sandstone and shale by combining typical V–ϕ trajectories and exponential ϕ–z relationships that are constrained by the critical porosity of the sediment at the surface and have shown that:

- The concave V–ϕ path for sandstone with initial grain contact leads to a monotonous decrease in the velocity gradient with depth. Therefore, V–z trends for consolidated sandstone have often been approximated by power-law V–z trends with the velocity gradient decreasing monotonously with depth, a formulation that predicts zero velocity at the surface and infinite velocity at depth. We present a

constrained V–z trend for sandstone, based on a modified Voigt model (equation (A2)), and, as an approximation to this trend – a constrained, exponential V–z trend, based on a modified velocity-average equation (equation (B2)).

- The convex V–ϕ path of lithologies such as shale or chalk that are initially compliant may lead to a maximum velocity gradient at some intermediate depth before the gradient approaches zero. V–z trends for marine shale have thus often been approximated by exponential tt–z trends for which the velocity gradient increases (towards infinity) with depth. We suggest a constrained exponential tt–z model (equation 5), based on a modified time-average equation (equation (B1)), as other workers have done before us.

Different velocity-depth gradients for shale and sandstone lead to a considerable range of velocities for these lithologies at a burial depth of 1 to 2 km (normal compaction). Estimates of maximum burial (and hence exhumation) should be based on velocities for specific lithologies: depth of normal compaction may vary up to 1 km depending on whether the lithology is assumed to be shale or sand.

The case study of baselines for sandstone and shale in the North Sea underlines the importance of applying constrained models and also the difficulty of estimating such trends when the sediments are not at maximum burial due to exhumation. The baseline for the redbeds of the Triassic Bunter Shale and Sandstone is found to be in agreement with the modified Voigt model for sandstone, assuming that the onset of quartz cementation occurs below a depth of approximately 2 km. The baseline for marine shale agrees with the shale trends of previous workers, and it can be applied to predict overpressure from sonic data.

Normal velocity–depth trends derived from basinwide data thus give us the opportunity to study the rock physical behaviour of different lithologies under natural conditions that may be difficult to imitate in the laboratory.

ACKNOWLEDGEMENTS

The financial support from the Carlsberg Foundation, GEUS and Stanford Rock and Borehole Geophysics Project is gratefully acknowledged. The constructive comments of reviewers, editors, J.A. Chalmers and J. Ineson improved the paper, which has been published with permission of the Geological Survey of Denmark and Greenland.

REFERENCES

Acheson C.H. 1963. Time-depth and velocity-depth relations in western Canada. *Geophysics* **28**, 894–909.

Al-Chalabi M. 1997a. Instantaneous slowness versus depth functions. *Geophysics* **62**, 270–273.

Al-Chalabi M. 1997b. Time-depth relationships for multilayer depth conversion. *Geophysical Prospecting* **45**, 715–720.

Athy L.F. 1930. Compaction and oil migration. *American Association of Petroleum Geologists Bulletin* **14**, 25–35.

Bertelsen F. 1980. Lithostratigraphy and depositional history of the Danish Triassic. *Geological Survey of Denmark*. Series B, 4. Geological Survey of Denmark.

Bjørlykke K. and Egebjerg P.K. 1993. Quartz cementation in sedimentary basins. *American Association of Petroleum Geologists Bulletin* **77**, 1538–1548.

Bulat J. and Stoker S.J. 1987. Uplift determination from interval velocity studies, UK, southern North Sea. In: *Petroleum Geology of Northwest Europe* (eds J. Brooks and K. W. Glennie), pp. 293–305. Graham & Trotman.

Chapman R.E. 1983. *Petroleum Geology*. Elsevier. Science Publishing Co.

Chen Q. and Nur A. 1994. Critical concentration models for porous materials. In: *Advances in Porous Media* (ed. M. Y. Corapcioglu), pp. 169–308. Elsevier. Science Publishing Co.

Corcoran D.V. and Doré A.G. 2005. A review of techniques for the estimation of magnitude and timing of exhumation in offshore basins. *Earth-Science Reviews* **72**, 129–168.

Corcoran D.V. and Mecklenburgh R. 2005. Exhumation of the Corrib gasfield, Slyne Basin, offshore Ireland. *Petroleum Geoscience* **11**, 239–256.

Dvorkin J., Gutiérrez M.A. and Nur A. 2002. On the universality of diagenetic trends. *The The Leading Edge* **21**, 40–43.

Dvorkin J. and Nur A. 1996. Elasticity of high-porosity sandstones – theory for two North Sea data sets. *Geophysics* **61**, 1363–1370.

Fabricius I.L. 2003. How burial diagenesis of chalk sediments controls sonic velocity and porosity. *American Association of Petroleum Geologists Bulletin* **87**, 1755–1778.

Faust L.Y. 1951. Seismic velocity as a function of depth and geologic time. *Geophysics* **16**, 192–206.

Feng S. and Sen P.N. 1985. Geometrical model of conductive and dielectric properties of partially saturated rocks. *Journal of Applied Physics* **58**, 3236–3243.

Greenberg M.L. and Castagna J.P. 1992. Shear-wave velocity estimation in porous rocks: Theoretical formulation, preliminary verification and applications. *Geophysical Prospecting* **40**, 195–209.

Guéguen Y., Chelidze T. and Le Ravalec M. 1997. Microstructures, percolation thresholds, and rock physical properties. *Tectonophysics* **279** (1–4), 23–35.

Guéguen Y. and Palciauskas V. 1994. *Introduction to the Physics of Rocks*. Princeton University Press.

Han D.H., Nur A. and Morgan D. 1986. Effects of porosity and clay content on wave velocities in sandstones. *Geophysics* **51**, 2093–2107.

Hansen S. 1996a. A compaction trend for Cretaceous and Tertiary shales on the Norwegian Shelf based on sonic transit times. *Petroleum Geoscience* **2**, 159–166.

Hansen S. 1996b. Quantification of net uplift and erosion on the Norwegian Shelf south of 66°N from sonic transit times of shale. *Norsk Geologisk Tidsskrift* **76**, 245–252.

Haskell N.A. 1941. The relation between depth, lithology, and seismic wave velocity in Tertiary sandstones and shales. *Geophysics* **6**, 318–326.

Heasler H.P. and Kharitonova N.A. 1996. Analysis of sonic well logs applied to erosion estimates in the Bighorn Basin. *Wyoming. American Association of Petroleum Geologists Bulletin* **80**, 630–646.

Hillis R.R. 1995. Quantification of Tertiary exhumation in the United Kingdom southern North Sea using sonic velocity data. *American Association of Petroleum Geologists Bulletin* **79**, 130–152.

Hottmann C.E. and Johnson R.K. 1965. Estimation of formation pressures from log-derived shale properties. *Journal of Petroleum Technology* **17**, 717–723.

Issler D.R. 1992. A new approach to shale compaction and stratigraphic restoration, Beaufort-Mackenzie Basin and Mackenzie Corridor, northern Canada. *American Association of Petroleum Geologists Bulletin* **76**, 1170–1189.

Japsen P. 1993. Influence of lithology and Neogene uplift on seismic velocities in Denmark; implications for depth conversion of maps. *American Association of Petroleum Geologists Bulletin* **77**, 194–211.

Japsen P. 1998. Regional velocity-depth anomalies, North Sea Chalk. A record of overpressure and Neogene uplift and erosion. *American Association of Petroleum Geologists Bulletin* **82**, 2031–2074.

Japsen P. 1999. Overpressured Cenozoic shale mapped from velocity anomalies relative to a baseline for marine shale, North Sea. *Petroleum Geoscience* **5**, 321–336.

Japsen P. 2000. Investigation of multi-phase erosion using reconstructed shale trends based on sonic data. Sole Pit axis, North Sea. *Global and Planetary Change* **24**, 189–210.

Johnson H., Warrington G. and Stoker S.J. 1994. 6. Permian and Triassic of the southern North Sea. In: *Lithostratigraphic Nomenclature of the UK North Sea* (eds R. W. O'B. Knox and W. G. Cordey). British Geological Survey.

Lander R.H. and Walderhaug O. 1999. Predicting porosity through simulating sandstone compaction and quartz cementation. *American Association of Petroleum Geologists Bulletin* **83**, 433–449.

Liu G. and Roaldset R. 1994. A new decompaction model and its application to the northern North Sea. *First Break* **12**, 81–89.

Magara K. 1976. Thickness of removed sedimentary rocks, paleopore pressure, and paleotemperature, southwestern part of Western Canada Basin. *American Association of Petroleum Geologists Bulletin* **60**, 554–565.

Magara K. 1978. Compaction and Fluid Migration. *Practical Petroleum Geology*. Elsevier. Science Publishing Co.

Mackay L.M. and White N.J. 2006. Accurate estimates of the spatial pattern of denudation by inversion of stacking velocity data: An example from the British Isles. *Geochemistry, Geophysics and Geosystems 7*, Q10007, 1–34.

Marion D., Nur A., Yin H. and Han D. 1992. Compressional velocity and porosity in sand-clay mixtures. *Geophysics* **57**, 554–563.

Mavko G., Mukerji T. and Dvorkin J. 1998. *The Rock Physics Handbook*. Cambridge University Press.

Michelsen O. 1989. Revision of the Jurassic lithostratigraphy of the Danish subbasin. Geological Survey of Denmark, Copenhagen.

Nolen-Hoeksema R.C. 1993. Porosity and consolidation limits of sediments and Gassmann's elastic-wave equation. *Geophysical Research Letters* **20**, 847–850.

Nur A., Marion D. and Yin H. 1991. Wave velocities in sediments. In: *Shear Waves in Marine Sediments* (ed. J. M. Hovem), pp. 131–140. Kluwer. Academic Publishers.

Nur A., Mavko G., Dvorkin J. and Galmundi D. 1998. Critical porosity; a key to relating physical properties to porosity in rocks. *The The Leading Edge* **17**, 357–362.

Olsen R.C. 1979. Lithology. Well 17/10—1. NPD Paper 21.

Osborne M.J. and Swarbrick R.E. 1997. Mechanisms for generating overpressure in sedimentary basins. *A Re–Evaluation. American Association of Petroleum Geologists Bulletin* **81**, 1023–1041.

Pryor W.A. 1973. Permeability-porosity patterns and variations in some Holocene sand bodies. *American Association of Petroleum Geologists Bulletin* **57**, 162–189.

Raymer L.L., Hunt E.R. and Gardner J.S. 1980. An improved sonic transit time-to-porosity transform. Proceedings of SPWLA 21 Annual Logging Symposium, pp. 1–12.

Rolle F. 1985. Late Cretaceous-Tertiary sediments offshore central West Greenland: lithostratigraphy, sedimentary evolution, and petroleum potential. *Canadian Journal of Earth Science* **22**, 1001–1019.

Rubey W.W. and Hubbert M.K. 1959. Role of fluid pressure in mechanics of overthrust faulting, II. *Geological Society America Bulletin* **70**, 167–206.

Scherbaum F. 1982. Seismic velocities in sedimentary rocks; indicators of subsidence and uplift. *Geologische Rundschau* **71**, 519–536.

Scholle P.A. 1977. Chalk diagenesis and its relation to petroleum exploration; oil from chalks, a modern miracle? *American Association of Petroleum Geologists Bulletin* **61**, 982–1009.

Sclater J.G. and Christie P.A.F. 1980. Continental stretching; an explanation of the post-Mid-Cretaceous subsidence of the central North Sea basin. *Journal of Geophysical Research* **85**, 3711–3739.

Serra O. 1986. *Fundamentals of Well-Log Interpretation*. Elsevier. Science Publishing Co.

Slotnick M.M. 1936. On seismic computations, with applications, II. *Geophysics* **1**, 299–305.

Smith T. and Sondergeld C.H. 2001. Examination of AVO response in the eastern deepwater Gulf of Mexico. *Geophysics* **66**, 1864–1876.

Snieder R., Xie M.Y., Pica A. and Tarantola A. 1989. Retrieving both the impedance contrast and background velocity. A global strategy for the seismic reflection problem. *Geophysics* **54**, 991–1000.

Terzaghi K. and Peck R.P. 1968. *Soil Mechanics in Engineering Practice*. John Wiley & Sons, Inc.

Walford H.L. and White N.J. 2005. Constraining uplift and denudation of west African continental margin by inversion of stacking velocity data. *Journal of Geophysical Research-Solid Earth* **110**, B04403, 1–16.

Ware P.D. and Turner J.P. 2002. Sonic velocity analysis of the Tertiary denudation of the Irish Sea basin. In: *Exhumation of the North Atlantic Margin: Timing, Mechanisms and Implications for Petroleum Exploration*, 196 (eds A. G. Doré, J. A. Cartwright, M. S. Stoker, J. P. Turner, N. White), pp. 355–370. Geological Society.

Weaver C.E. 1989. *Clays, Muds and Shales*. Elsevier. Science Publishing Co.

Winthaegen P.L.A. and Verweij J.M. 2003. Estimating regional pore pressure distribution using 3D seismic velocities in the Dutch Central North Sea Graben. *Journal of Geochemical Exploration* **78–79**, 203–207.

Wyllie M.R.J., Gregory A.R. and Gardner L.W. 1956. Elastic wave velocities in heterogeneous and porous media. *Geophysics* **21**, 41–70.

APPENDIX A

Bounds on velocity

The simplest bounds on velocity are the Voigt and Reuss bounds (cf. Mavko *et al*. 1998). The Voigt upper bound of the effective elastic modulus, M_V, of N phases is

$$M_v = \sum_{i=1}^{N} f_i M_i,$$

where f_i is the volume fraction and M_i is the elastic modulus of the ith phase (either bulk modulus $K = \rho(V_p^2 - 4/3V_s^2)$ [GPa], P-wave modulus $M = \rho V_p^2$, or shear modulus $\mu = \rho V_s^2$, where the density of the rock is $\rho = (1-\phi)\rho_m + \phi\rho_{fl}$ [g/cm ^{3}], ρ_m is density of the mineral material, ρ_{fl} is the fluid density, V_P and V_S are the P- and S-wave velocities [km/s]). The Reuss lower bound of the effective elastic modulus, M_R is given by

$$\frac{1}{M_R} = \sum_{i=1}^{N} f_i \frac{1}{M_i}$$

The Reuss average describes exactly the effective moduli of a suspension of solid grains in a fluid. In the suspension domain, $\phi > \phi_c$, the effective bulk and shear moduli can be estimated quite accurately using the Reuss (iso-stress) average:

$$K_R^{-1} = (1-\phi)K_m^{-1} + \phi K_{fl}^{-1}, \quad \mu_R = 0, \tag{A1}$$

where K_m and K_{fl} are the bulk moduli of the mineral material and the fluid. The effective shear modulus of the suspension is zero, because the shear modulus of the fluid is zero. We can thus calculate the P-wave velocity V_c at ϕ_c where the mineral grains are barely touching ($\mu_c = 0$):

$$V_c = \sqrt{(K_c + 4/3\mu_c)/\rho_c} = \sqrt{K_c/\rho_c},$$

where the subscript c indicates the value at critical porosity: $K_c^{-1} = (1-\phi_c)K_m^{-1} + \phi_c K_{fl}^{-1}$ and $\rho_c = (1+\phi_c)\rho_m + \phi_c \rho_{fl}$.

A linear trend of ρV^2 versus ϕ may be used to describe the compaction trend for clean sandstones at high effective pressure, leading to convenient mathematical properties (Nur *et al*. 1991; Marion *et al*. 1992). This linear dependence can be thought of as a modified Voigt average:

$$M_{MV} = (1-\phi')M_m + \phi' M_c, \tag{A2}$$

where M_m and M_c are the moduli (bulk or shear) of the mineral material at zero porosity and of the suspension at the critical porosity (M_c is given by equation (A1) with $\phi = \phi_c$). The expression is modified in the sense that the porosity is scaled by the critical porosity $\phi' = \phi/\phi_c$, so that ϕ' ranges from 0 to 1 as ϕ ranges from 0 to ϕ_c. If the low-porosity end-member is taken as the porosity at finite depth, ϕ_{fin}, rather than 0, to fit data from sedimentary basins, we have $\phi' = (\phi - \phi_{fm})(\phi_c - \phi_{fm})$. Note that using the suspension modulus M_c in this form automatically incorporates the effect of pore fluids on the modified Voigt average. The modified Voigt average (equation (A2)) can be transformed into a velocity–depth model by calculating porosity as a function of depth by assuming exponential porosity decay (equation 2). The appropriate rock physical properties for sandstone with 0, 10, 20 and 30% clay content, based on data from Han *et al*. (1986), are given in Table 1(b) and for the ϕ–z model for sandstone in Table 1(a).

APPENDIX B

V–z relationships for specific V–ϕ trends

Transit time proportional to ϕ^{α_t} (modified time-average equation)

Let transit time be dependent on porosity raised to the power of a positive constant α_t:

$$tt = (tt_c - tt_m)\left(\frac{\phi}{\phi_c}\right)^{\alpha_t} + tt_m \Rightarrow \ln\left(\frac{tt - tt_m}{tt_c - tt_m}\right) = \alpha_t \ln\left(\frac{\phi}{\phi_c}\right),$$

where tt_m is the transit time of the matrix and tt_c is that of the rock at critical porosity (the simple time-average for a rock is given by $(1-\phi)tt_m + \phi tt_{fl}$). We see that transit time varies between tt_c and tt_m for ϕ varying between ϕ_c and 0%, and that $(tt–tt_m)$ and ϕ are plotted as a straight line on a log-log plot. The V–ϕ path for this relationship is convex for all positive values of α_t. We get a linear $\ln(tt–tt_m)$–z function similar to equation (C5) by substituting the exponential ϕ–z function with decay rate β (equation 2):

$$tt = (tt_c - tt_m)e^{-z/b_2} + tt_m \Rightarrow \ln(tt - tt_m) = \ln(tt_c - tt_m) - \frac{z}{b_2},$$

where $b_2 = \beta/\alpha_t$. Conversely, we see that the above V–z trend implies that transit time is proportional to $(\phi/\phi_c)^{\beta/b_2}$ if porosity decays exponentially with depth.

If the decay rates of ϕ and tt are identical, $\beta = b_2$, we have linearity between tt and ϕ ($\alpha_t = 1$), and we get a modified

time-average equation:

$$tt = (tt_c - tt_m)\phi/\phi_c + tt_m. \quad \text{(B1)}$$

This equation should be compared with the Wyllie *et al.* (1956) time-average equation that states proportionality between transit time and porosity (tt_{fl} is the transit time of the pore fluid):

$$tt = (tt_{fl} - tt_m)\phi + tt_m,$$

where $\phi = 1$ is taken as maximum porosity (and not ϕ_c), and the velocity at maximum porosity equals V_{fl} (and not V_c) (equation (A1)). The constrained transit-time–depth trend of equation (C5) can thus be derived by combining the modified time-average equation with the assumption of exponential decay of porosity (equations (B1) and (2)).

Velocity proportional to ϕ^{α_v} (modified velocity-average equation)

Let velocity be dependent on porosity raised to the power of a positive constant α_v:

$$V = V_m - (V_m - V_c)\left(\frac{\phi}{\phi_c}\right)^{\alpha_v}$$
$$\Rightarrow \ln(V_m - V) = \ln(V_m - V_c) + \alpha_v \ln\left(\frac{\phi}{\phi_c}\right),$$

where V_m is the velocity of the matrix and V_c is that of the rock at critical porosity (the simple velocity-average for a rock is defined as $(1–\phi)V_m + \phi V_{fl}$). We see that velocity varies between V_c and V_m for ϕ varying between ϕ_c and 0%, and that $(V_m - V)$ and ϕ are plotted as a straight line in a log-log plot. The V–ϕ path is concave for $\alpha_v > 1$ ($d^2V/d\phi^2 < 0$), and convex for $0 < \alpha_v < 1$, while it is a straight line for $\alpha_v = 1$ (a modified velocity-average). We get the following linear $\ln(V_m - V)$–z trend by substituting the exponential ϕ–z function with decay rate β (equation 2):

$$V = V_m - (V_m - V_c)e^{-z/b_3}$$
$$\Rightarrow \ln(V_m - V) = \ln(V_m - V_c) - \frac{z}{b_3}, \quad \text{(B2)}$$

where $\beta_3 = \beta/\alpha_v$. In the special case where $\alpha_v = 1$, velocity becomes linearly proportional to porosity and $b_3 = \beta$. The trend is a constrained velocity–depth model for which the velocity gradient decreases monotonously with depth for all values of b_3 and thus, even for convex V–ϕ paths ($0 < \alpha_v < 1$), there is no maximum velocity–depth gradient at intermediate depths.

We can estimate the parameters in equation (B2) as an approximation to the modified Voigt trend (equation (A2)) for $z < 4$ km taking $V_c = 1600$ m/s; for sandstone with varying clay content, we get

0% clay: $V_m = 5065$ m/s, $b_3 = 1923$m,
5% clay: $V_m = 4796$ m/s, $b_3 = 1963$m,
10% clay: $V_m = 4526$ m/s, $b_3 = 2003$m,
20% clay: $V_m = 4288$ m/s, $b_3 = 2042$m,
30% clay: $V_m = 4056$ m/s, $b_3 = 2076$m.

The depth predicted by these approximations deviates less than 90 m from the respective Voigt model for a given velocity and this is considered insignificant. The model for 5% clay corresponds to the normal velocity–depth trend for the redbeds of the Triassic Bunter Shale and Sandstone formations ($V > 3.6$ km/s; see Figs 6 and 7)

APPENDIX C

Review of analytical formulations of V–z trends

Several functions have been applied to represent the increase in velocity with depth (Table 2). A linear velocity–depth function has been used by several workers for different lithologies (e.g. Slotnick 1936; Bulat and Stoker 1987; Japsen 1993):

$$V = V_0 + kz, \quad \text{(C1)}$$

where the velocity–depth gradient k is positive (curve B&S in Fig. 10).

Hillis (1995) applied a linear function between transit time and depth for chalk, sandstone and shale:

$$tt = tt_0 + qz, \quad \text{(C2)}$$

where tt_0 is the transit time at the surface and q [μs/m^2] is the negative transit-time–depth gradient (cf. Al-Chalabi 1997a; curve H in Fig. 10).

Velocity–depth relationships for shale have often been approximated by a simple exponential model for the reduction of transit time with depth (e.g. Hottmann and Johnson 1965; Magara 1978; Hansen 1996b):

$$tt = tt_0 e^{-z/b_1} \Rightarrow \ln(tt) = \ln(tt_0) - z/b_1, \quad \text{(C3)}$$

where b_1 [m] is an exponential decay constant (curve Ha in Fig. 4).

Acheson (1963) found that velocity in sedimentary basins was proportional to depth raised to the power of (1–n):

$$V = dz^{1-n}, \Rightarrow \ln(V) = \ln(d) + (1 - n)\ln(z), \quad \text{(C4)}$$

where n is a number between 0.83 and 1, and d [m^n/s] is a coefficient. The velocity at the surface is predicted to be zero,

so the expression is only valid below a certain depth. Similar formulations were applied by Faust (1951).

The above four formulations are linear relationships in the V–z, tt–z, ln(tt)–z and ln(V)–ln(z) planes, respectively. While they may be valid approximations within a given interval, they all predict that velocity approaches infinity at depth. Only the power-law V–z trend (equation (C4)) predicts that the velocity gradient decreases with depth; the linear V–z trend (equation (C1)) has a constant gradient, and the linear tt–z and the exponential tt–z trends (equations (C2) and (C3)) have increasing gradients with depth. However, we have shown that an increasing velocity gradient at shallow depths characterizes initially compliant sediments, whereas the velocity gradient for initially stiff rocks decreases with depth. This point explains why the linear tt–z and exponential tt–z trends have been applied so successfully to initially compliant rocks, like chalk and shale (e.g. Hottmann and Johnson 1965; Hillis 1995), and why the power-law V–z model has been applied primarily to sand-shale sequences (e.g. Faust 1951; Acheson 1963).

A constrained exponential transit-time–depth model was suggested for shale by Chapman (1983), and applied for sand/shale series by Heasler and Kharitonova (1996) and for Triassic redbeds by Ware and Turner (2002):

$$tt = (tt_0 - tt_\infty)e^{-z/b_2} + tt_\infty$$
$$\Rightarrow \ln(tt - tt_\infty) = -z/b_2 \ln(tt_0 - tt_\infty), \quad \text{(C5)}$$

where tt_∞ is the transit time at infinite depth and b_2 [m] is an exponential decay constant (cf. Al-Chalabi 1997a). This model predicts finite values of transit time at the surface and at infinite depth, i.e. tt_0 and tt_∞, respectively. This formulation is linear in the ln $(tt - tt_\infty) - z$ plane, and implies that $k \to 0$ for $z \to \infty$. The velocity gradient for this V–z trend has a maximum for $z = b_2 \ \ln [(tt_0 - tt_\infty)/tt_\infty]$. This model may thus be applied to initially compliant rocks, such as shale (e.g. Chapman 1983), or more specifically to marine shale dominated by smectite/illite (equation 5; curve V_N^{sh} in Fig. 4) (Japsen 1999, 2000).

Segmented linear velocity–depth functions have been suggested for the North Sea chalk (Upper Cretaceous-Danian) and for the Triassic Bunter Shale because no single mathematical function matched the observed trends (Japsen 1998, 2000). Such continuous and non-linear functions are defined over a velocity interval divided into n segments:

$$V = V_{0i} + k_i z, \quad z_{ai} < z < z_{bi}, \quad \text{(C6)}$$

where V_{0i} and k_i are the velocity at the surface and the velocity–depth gradient of the ith segment defined for velocities between V_{ai} and V_{bi}. The shift of the velocity gradient between the segments reflects variations in the compaction process (Japsen 1998).